*Biology of Reproduction,* 2021, 1–12
doi:10.1093/biolre/ioab005
Research Article

OXFORD

Research Article

# Metabolomic differences in blastocoel and uterine fluids collected in vivo by ultrasound biomicroscopy on rabbit embryos†

**Sophie Calderari[1,2,*], Nathalie Daniel[1,2], Eve Mourier[1,2,3], Christophe Richard[1,2,3], Michele Dahirel[1,2,3], Franck Lager[4], Carmen Marchiol[4], Gilles Renault[4], Julie Gatien[5], Lydie Nadal-Desbarats[6,7], Pascale Chavatte-Palmer[1,2,3,‡] and Véronique Duranthon[1,2,‡]**

[1]Université Paris-Saclay, UVSQ, INRAE, BREED, Jouy-en-Josas, France, [2]Ecole Nationale Vétérinaire d'Alfort, BREED, Maisons-Alfort, France, [3]Plateforme MIMA2-CIMA, Jouy en Josas, France, [4]INSERM U1016, Institut Cochin, Université Paris Descartes, PRES Sorbonne Paris Cité, Paris, France, [5]Research and Development Department, Allice, Nouzilly, France, [6]UMR 1253, iBrain, Inserm, University of Tours, Tours, France and [7]PST-ASB, University of Tours, Tours, France

*__Correspondence:__ INRAE UMR 1198 BREED, Domaine de Vilvert, Bat 230, 78350, Jouy-en-Josas, France.
Tel: +33 1 34 65 20 75; E-mail: sophie.calderari@inrae.fr

†__Grant Support__: This work was supported by INRAE with dedicated help from the INRAE PhASE department (CI 2014 and CI 2015).
‡These two authors contributed equally to this study.

Received 20 August 2020; Revised 24 November 2020; Accepted 7 January 2021

## Abstract

The success of embryo development and implantation depends in part on the environment in which the embryo evolves. However, the composition of the uterine fluid surrounding the embryo in the peri-implantation period remains poorly studied. In this work, we aimed to develop a new strategy to visualize, collect, and analyze both blastocoelic liquid and juxta-embryonic uterine fluid from in vivo peri-implantation rabbit embryos. Using high-resolution ultrasound biomicroscopy, embryos were observed as fluid-filled anechoic vesicles, some of which were surrounded by a thin layer of uterine fluid. Ultrasound-guided puncture and aspiration of both the blastocoelic fluid contained in the embryo and the uterine fluid in the vicinity of the embryo were performed. Using nuclear magnetic resonance spectroscopy, altogether 24 metabolites were identified and quantified, of which 21 were detected in both fluids with a higher concentration in the uterus compared to the blastocoel. In contrast, pyruvate was detected at a higher concentration in blastocoelic compared to uterine fluid. Two acidic amino acids, glutamate and aspartate, were not detected in uterine fluid in contrast to blastocoelic fluid, suggesting a local regulation of uterine fluid composition. To our knowledge, this is the first report of simultaneous analysis of blastocoelic and uterine fluids collected in vivo at the time of implantation in mammals, shedding new insight for understanding the relationship between the embryo and its local environment at this critical period of development.

**Summary sentence:** Development of an innovative technique coupling ultrasound biomicroscopy, guided puncture, and nuclear magnetic resonance to characterize the in vivo uterine and blastocoelic microenvironment of the peri-implantation rabbit embryo.

## Graphical Abstract

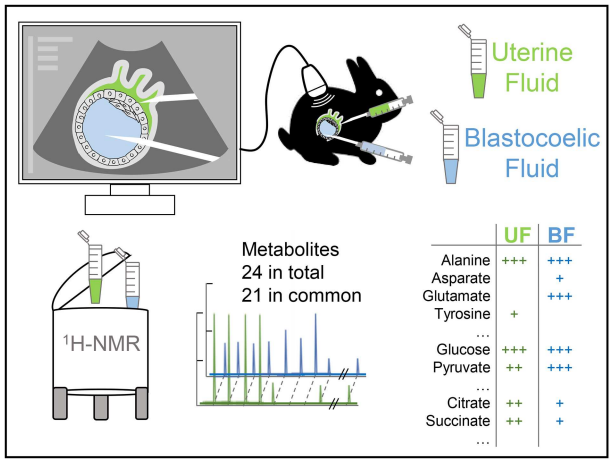


**Key words**: pre-implantation embryo, rabbit, blastocoel, uterine fluid, ultrasound biomicroscopy, metabolite.

## Introduction

The use of assisted reproductive technology (ART) has increased over the last decades, with ART infants representing nowadays more than 2.3% of birth in Europe [1]. Despite a great improvement in embryo transfer procedures, the pregnancy rate remains low, with 25% of transfers resulting in a birth [1]. The last years have been characterized by a marked increase of a single embryo transferred per cycle (representing 25.6% of treatment cycles in 2015 [1] as compared to 18.9% in 2005 in Europe [2]) to avoid multiple pregnancies. Thus, the selection of the embryo with the highest chances for implantation is the current challenge faced by reproductive biologists. The use of morphological evaluation and, more recently, morphokinetic criteria remains insufficient to predict successful implantation [3]. Strategies for identifying potential biological markers using omics technologies are being explored as alternative selection methods [4]. Among those, metabolomics studies are of major interest to identify biomarkers present in culture media in order to predict quality, viability, survival, and implantation potential of embryos [4, 5]. Promising and noninvasive, metabolomics enables the detection of the elements produced by the embryo and released into the culture medium. One of the major limitations is, however, the difficulty to discriminate between embryonic products and compounds originating from the culture medium [6]. The blastocoelic fluid may represent an alternative biological source for identifying biomarkers of embryo survival [7–10]. Currently, the use of vitrification for cryopreservation of human embryos is becoming widespread in human ART [1], with the blastocoelic fluid being discarded as a waste product [11]. Indeed, a previtrification artificial blastocyst shrinkage through blastocoelic fluid volume reduction has been developed to limit ice crystal formation and improved survival after warming [12, 13]. Proteins have been recently detected using mass spectrometry analyses in the blastocoelic fluid of in vitro produced human embryos [7–10], with more than a hundred proteins identified, mostly involved in metabolic process, developmental function, or immune response [7, 8, 10]. Although studies aiming at characterizing the blastocoelic fluid of the in vitro developed embryo are promising, knowledge about the blastocoelic fluid composition of in vivo embryos around the time of implantation is lacking.

The blastocoel cavity appears after compaction, when the embryo moves from the oviduct to the uterus. At this time, undifferentiated blastomeres begin to differentiate into the trophectoderm (TE) that encircles a small group of cells, the inner cell mass (ICM), and secrete fluid into the compacted embryo to create a fluid-filled cavity, the blastocoel. TE gives rise to placental tissues, and ICM gives rise to the developing embryo and can also be isolated to form pluripotent embryonic stem cells with the potential to develop in vitro into various lineages [14]. Mechanisms involved in the differentiation of the first cell lineages have been extensively characterized [15]. Paradoxically, the blastocoelic fluid composition remains poorly described. Its production relies on a ion gradient, resulting in influx of water from the external milieu to form the blastocoel cavity. This ion transport depends on the properties of the TE, mainly driven by $Na^+/K^+$-ATPase localized at the basolateral membrane of this epithelium [16]. Accumulation of blastocoelic fluid is dependent on epithelial junctional complex and cell-to-cell adhesion between TE cells [16]. The expression of transport systems in the apical and/or basolateral cell membranes of TE cells leads to a specific ion, amino acid, carbohydrate composition that differs from external milieu [17]. In addition to the transcellular transfer, ICM and TE cells release and secrete proteins [18].

The source for the formation of the blastocoelic fluid is the embryonic environment, first the oviductal fluid up to the early blastocyst stage and then the uterine fluid until implantation of the blastocyst [19]. Both the oviduct and the uterus are bordered by an epithelium that directly contributes to the formation of the oviductal and uterine fluid, respectively, together with the transudation from systemic maternal circulation [20]. Oviductal and uterine fluids' composition is complex [20] and the volume of each compartment varies according to the hormonal context, in order to facilitate embryo transport, development, and implantation [19, 21]. Moreover, these fluids' composition are also dynamic, with concentrations of nutrients such as pyruvate, lactate, glucose, lipids,

or amino acids but also of proteins varying throughout the oviduct, in response to the endocrine status and/or the presence of embryo [19–25]. A better knowledge of the composition of the uterine fluid in the peri-implantation period is of major interest to characterize the importance of this embryonic microenvironment and how it affects blastocoelic fluid composition, crucial both in vivo and in vitro for the conception of embryo culture media. Moreover, as successful embryo-uterus interaction requires a competent blastocyst to be transferred into the most receptive uterine environment, the analysis of uterine fluid seems to be an indispensable source of information to determine when the endometrium is more receptive to the embryo, defining the appropriate time for transfer.

Ultrasound biomicroscopy or micro-ultrasound allows ultrasound visualization of living tissue at microscopic resolution [26]. In biomedical research focused on pregnancy, this technology is used for noninvasive in utero imaging of live embryos, especially in small animals [27]. Indeed, since the demonstration of its first use on mouse embryos in 1995 [28], it has been widely used in mice to noninvasively detect implantation sites [29], determine gestational age [30], fetal resorption [27], and measure embryonic growth and organs development [27, 29, 31]. Ultrasound biomicroscopy is a real-time modality that can be used to guide in utero injections of cells, tracer dyes, and adenoviral or retroviral vectors [32–36]. Ultrasound biomicroscopy could represent a great tool to visualize the blastocyst and its microenvironment and to collect blastocoelic and uterine fluids, in particular in rabbits. Highly suitable animal model for studies in reproduction, the advantages of the rabbit model are numerous, both in terms of physiological and molecular considerations [37]. While the development of the rabbit embryo has been extensively studied, in vivo description of blastocyst development is scarce and characterizations were mainly performed by histology on postmortem specimen [38].

It becomes crucial to improve the knowledge of the in vivo composition of blastocoelic and uterine fluids during the peri-implantation period. In this work, we aimed to develop a new strategy to visualize, collect, and analyze both blastocoelic liquid and juxta-embryonic uterine fluid from peri-implantation rabbit embryos using ultrasound biomicroscopy and nuclear magnetic resonance (NMR) spectroscopy.

## Methods

### Ethics

Animal care and handling were carried out according to European regulations on animal welfare. The animal holding facilities were registered (agreement no. A78–3224 and A78–3221). EM, CR, ND, MD and SC have the authorization to work with laboratory animals from the departmental veterinary regulatory services. The local ethical committee (Comethea) approved the experimental design. The local ethical committee (Comethea, n°45 in French National register) approved the experimental design, which was registered under n°2015042115447836_v2.

### Animals

Ten New Zealand White female rabbits (INRA 1077 Line) were used. They were housed individually in one building maintained at 18–20 °C. The photoperiod was changed 1 week before artificial insemination from 8 to 16 h of light per day and was maintained at 16 h per day during the rest of the experiment. Does were artificially inseminated with two of five males of the same breed, used randomly. Ovulations were induced by an intramuscular injection of gonadorelin (GnRH), 0.05 mL/kg (Fertagyl, Merck, France).

Before surgery, the supports to hold and immobilize the embryonic vesicles were prepared (Figure 1). Petri dishes were cut on the side and a 1 cm diameter hole was cut out in the center of the dish, and covered with a thick latex membrane.

At 168 h post insemination, general anesthesia was performed in overnight fasted animals. Anesthesia was induced by intramuscular injection of xylazine (Rompun, Bayer, France) 0.05 mg/kg, ketamine (Imalgene, Merial, France) 0.11 mg/kg and butorphanol (Torbugesic, Zoetis, New Zealand) 0.05 mg/kg and anesthesia was maintained by inhalation of a mixture of 1–5% isoflurane and 1–1.5 L/min oxygen. Laparotomy was performed, and a small part of one uterine horn was externalized and covered by preheated ultrasound gel (Figure 2A, Supplementary Video 1). One embryonic vesicle was isolated, maintained static using the previously described customized holder and covered again by preheated ultrasound gel (Figure 2B, Supplementary Video 1). The ultrasound probe was positioned on the embryonic vesicle to visualize the vesicle in real time and guide the micropuncture. Micropuncture was performed using needle (30G, length 8 mm) and syringe (BD Micro-fine™+, BD, France) fixed on a micromanipulator and changed after each puncture (Figure 2C, Supplementary Video 1). The same procedure was repeated on all embryonic vesicles of the same horn. The uterine horn was then replaced in the abdomen, and the same procedure was repeated for the second uterine horn. After collecting fluids from all embryonic vesicles, the ultrasound gel was wiped off and uterine horns replaced into the abdomen. Ten milliliters of saline were injected into the abdominal cavity before suturing the abdominal wall and the skin. Total anesthesia never exceeded 2 h. Post-surgical analgesia was achieved by an intramuscular injection of 0.05 mL/kg of meloxicam (Metacam, Boehringer, Germany) and antibiotherapy was performed with a subcutaneous injection of 0.5 mL/kg oxytetracycline (Terralon 20% LA, Virbac, France) twice at 48-h intervals.

### Ultrasound biomicroscopy imaging and puncture

All images were obtained with a micro-ultrasound platform (Vevo2100, VisualSonics Inc, Toronto, Ontario, Canada) with the 70 MHz probe (MS-700). Providing a 30 micron resolution and frame rates up to 740 fps.

### Proton NMR spectroscopy measurements

Proton nuclear magnetic resonance ($^1$H-NMR) samples were prepared using 20 µL blastocoelic and uterine fluids diluted with 180 µL of 0.2 M potassium phosphate buffer in deuterium oxide. The entire diluted solution was then transferred to conventional 3-mm NMR tubes and spectra were recorded at 298 K on a Bruker Ascend 600-MHz spectrometer equipped with a TCI cryoprobe (Triple resonance Cryoprobe for Inverse detection). Standard NMR spectra were obtained using a "cpmgpr1d" pulse sequence with a relaxation delay of 25 s, number of scans of 256 on a time domain of 64 K data points. Water suppression was achieved by presaturation during the relaxation delay. Data were processed with 0.2-Hz line broadening for the exponential decay function using TopSpin version 3.2 software (Bruker Daltonik). Spectral assignments were done using the free version of ChenomX 7.1 (ChenomX Inc., Edmonton, Canada), an in-house database, and the human metabolome database (HMDB; http://www.hmdb.ca/). Metabolite quantifications using the Electronic Reference To access In vivo Concentrations (ERETIC) peak as a quantitative reference were obtained by the specific subroutine of

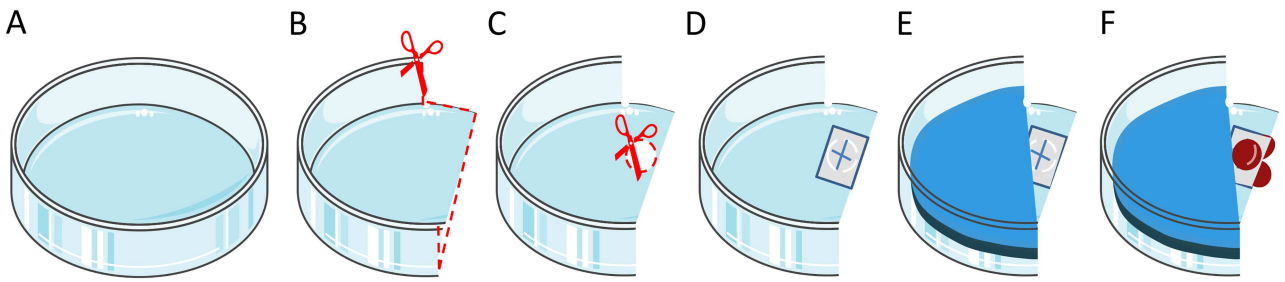


**Figure 1.** In-house manufacture of the embryonic vesicle support holder. (A) Petri dish. (B) The edges and the bottom are cut according to the dotted lines. (C) A 1 cm circle is cut in the bottom of the Petri dish, according to the dotted lines. (D) A piece of a thin latex membrane is placed over the hole, and a notch is made in this piece. (E) A half-disc of thick latex is placed on the intact part of the dish. (F) This customized support is placed on the externalized uterine tract; an embryonic vesicle is passed through the membrane to be gently immobilized. Covered with ultrasound gel, this vesicle is ready to be visualized.

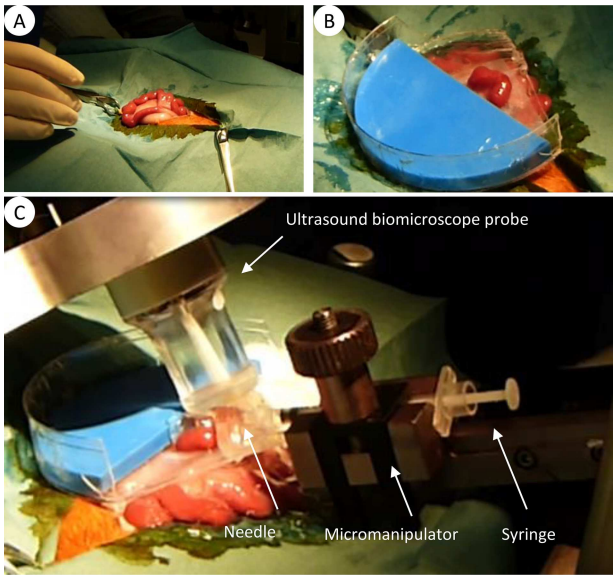


**Figure 2.** Positioning the ultrasound biomicroscope probe on rabbit embryonic vesicle. On an externalized part of uterine horn (A), one embryonic vesicle is maintained static using customized holder (B) to be accessible to visualization using ultrasound biomicroscope probe to collect fluids using needle/syringe fixed on a micromanipulator (C).

the Bruker TopSpin 3.2 program. The ERETIC signal was calibrated using a known solution. Metabolite quantification was not possible when the baseline was distorted by the presence of macromolecules, or the peaks of interest were overlapped with others. The spectral interval corresponding to the ultrasound gel was excluded from the analysis.

### Statistics

Differences between groups were compared using Wilcoxon signed rank test for paired samples. The data from blastocoelic and uterine fluids were analyzed by multivariate statistical data analysis, using MetaboAnalyst. Sample normalization was performed using the MetaboAnalyst procedure entitled "A pooled sample from group". In this procedure, an average of all blastocoelic fluids data was used to normalize the data set. The data were scaled using autoscaling mode (mean-centered and divided by the standard deviation of each variable) of MetaboAnalyst. The data were analyzed using principal component analysis (PCA), an unsupervised method and partial least squares discriminant analysis (PLS-DA), a supervised method. The overall quality of the models was judged by cumulative $R^2$ defined as the proportion of variance in the data explained by the model and cumulative $Q^2$, the class prediction ability of the model obtained by cross-validation.

## Results

### Ultrasound biomicroscopy imaging of the rabbit embryonic vesicle

As described in Methods, to make the embryonic vesicle accessible for a puncture, the uterine tract of anesthetized rabbit was externalized; one embryonic vesicle was isolated and stabilized on an in-house made uterine horn holder; and the ultrasound probe was positioned (Figure 2, Supplementary Video 1). Embryonic vesicles were observed using ultrasound biomicroscopy (Figure 3). The blastocoel was detected as a spherical hypoechogenic dark zone (Figure 3A and A′). The embryonic disk was positioned in the mesometrial side. The uterine cavity containing uterine fluid was detected next to the endometrial reaction on the mesometrial side (Figure 3A and A′). The different structures are schematized in Figure 3B.

Of 55 embryonic vesicles observed, 37 were spherical, very inflated, occupying the entire uterine space, with no detectable uterine cavity (Figure 3C). The entire vesicle was scanned and the maximum perimeter of each spherical blastocoelic cavity was measured. The mean perimeter of these spherical blastocoelic cavities was 15.0 mm ± 0.7 mm ($n$ = 24 embryos, from 8 rabbits). The remaining observed embryonic vesicles ($n$ = 18) were not as well swelled and the embryo was slightly (Figure 3D) or very collapsed (Figure 3E). In these collapsed embryos, the uterine cavity was detectable between the endometrium and the blastocyst (Figure 3D and E). In collapsed embryos, antimesometrial implantation sites could be identified as hyperechogenic zone in the endometrium (Figure 3E). In nine embryonic vesicles, mostly deflated, one or two small (<0.5 mm) hypoechogenic fluidic cavities were observed on the mesometrial side of the embryo (Figure 3F–H). They looked as if they were integrated in the lateral membrane of the embryo, the embryonic disk.

### Blastocoelic and uterine fluids puncture using ultrasound biomicroscopy

Using real-time ultrasound biomicroscopy images for guidance (Figure 4, Supplementary Videos 2–4), the needle tip was inserted

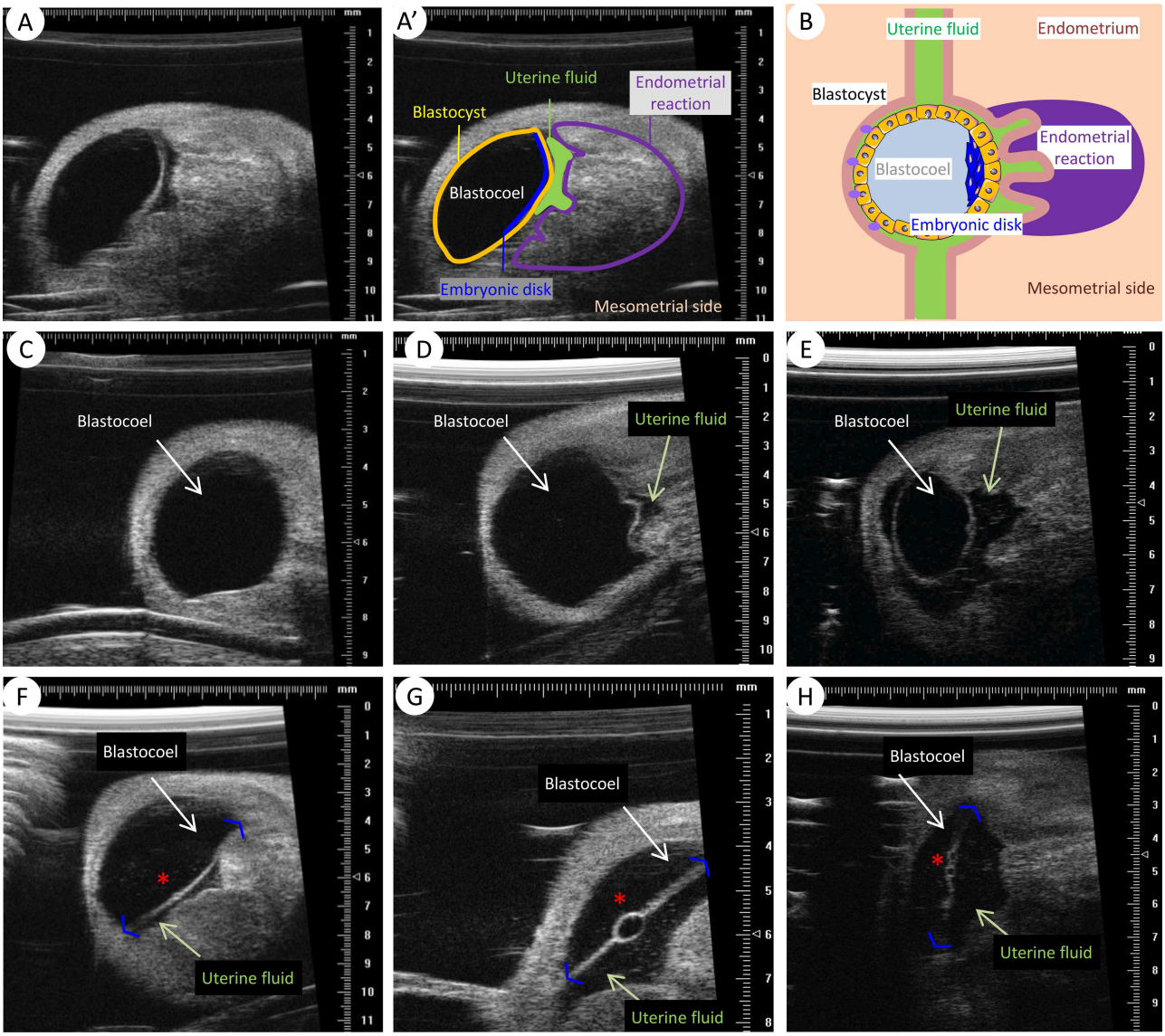


**Figure 3.** Ultrasound biomicroscopic images of rabbit embryonic vesicle. (A, B) Ultrasound biomicroscopic images of one embryonic vesicle in A, legended in A′, and schematized in B. (C–E) Embryonic vesicle with a very inflated embryo and no detectable uterine cavity in C, a less inflated embryo and the detection of a small uterine cavity in D, and a collapsed embryo with a large uterine cavity in E. (F–H) Detection of hypoechogenic fluidic cavities (red asterisk), one in F and G and two in H, on the mesometrial side of the embryo.

through the uterus. Depending on the position of the embryo in the embryonic vesicle, the turgidity of the blastocoelic cavity, and the visibility of the uterine cavity, the needle was oriented for a penetration either directly into the blastocoelic cavity to collect the blastocoelic liquid (Figure 4A, Supplementary Video 2) or into the uterine cavity in the vicinity of the embryo to collect the uterine fluid (Figure 4B, Supplementary Video 3). Fifty embryonic vesicles were punctured in 10 rabbits (Table 1). In 20 embryos, both the blastocoelic and the uterine fluids were successively collected, the uterine cavity became accessible for puncturing after blastocoelic puncture ($n$ = 18), or the blastocoelic cavity became accessible for puncturing after uterine puncture ($n$ = 2) (Table 1, Figure 4C, Supplementary Video 4). For 14 embryos, mainly well-inflated embryos, only the blastocoelic liquid was collected (5–60 µL) (Table 1, Figure 4A, Supplementary Video 2). For 16 embryos, rather collapsed embryos, only the uterine fluid was collected (5–60 µL) (Table 1, Figure 4B, Supplementary Video 3). Blood taint was observed in three blastocoelic liquids and in six uterine fluids (Table 1). The penetration of needle induced collapsing of the embryo in three cases. The collection of fluid induced an aspiration of the embryonic vesicle in three cases.

## Metabolomic profiling of blastocoelic and uterine fluids using $^{1}$H-NMR

$^{1}$H-NMR metabolomic profiling was conducted on blastocoelic and uterine fluids collected sequentially on the same embryonic vesicle, punctured from uncollapsed embryo, and exempt from blood. Fluids from seven embryos (7 blastocoelic fluids and 7 uterine fluids) collected from four different does were profiled. Blastocoelic and uterine fluids were profiled using the same NMR sequence, to allow comparison between fluids.

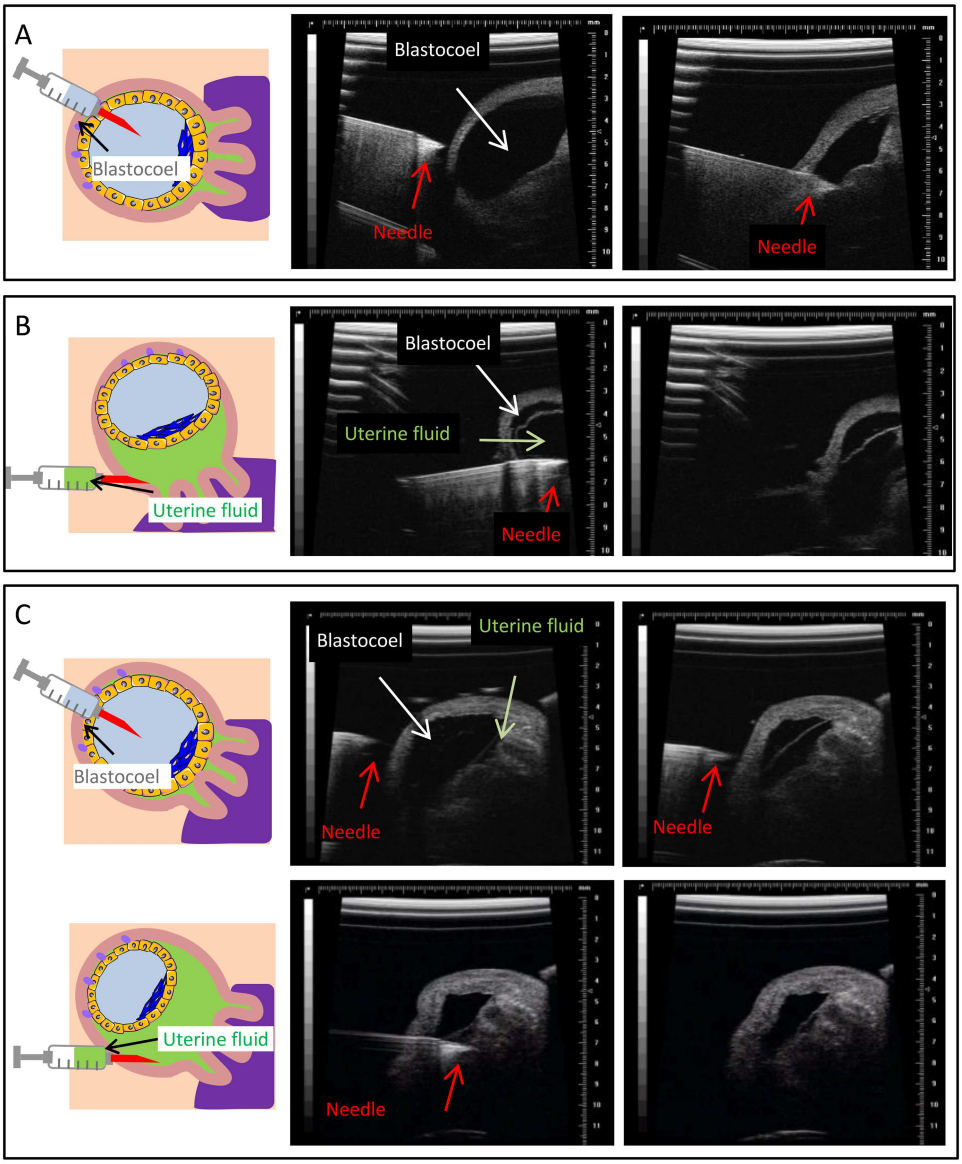


**Figure 4.** Blastocoelic and uterine fluids puncture using ultrasound biomicroscopy. (A) Blastocoelic fluid puncture. (B) Uterine fluid puncture. (C) Blastocoelic fluid and then uterine fluid puncture. For each panel, on the left is represented a schematic view of the collected fluid, on the middle the cavity before puncture, and on the right the cavity after puncture.

**Table 1.** Number and category of collected fluids.

| Cavity punctured | Number of embryonic vesicles | Number of uncollapsed embryos (% of embryonic vesicles) | Number of samples | | |
|---|---|---|---|---|---|
| | | | Total | Without blood taint (% of Total) | With blood taint (% of Total) |
| Blastocoelic only | 14 | 12 (86%) | 14 | 12 (86%) | 2 (14%) |
| Uterine only | 16 | 6 (37%) | 16 | 13 (81%) | 3 (19%) |
| Blastocoelic and Uterine | 20 | 18 (90%) | 20<br>20 | 19 (95%)<br>17 (85%) | 1 (5%)<br>3 (15%) |
| Total<br>*Blastocoelic liquid*<br>*Uterine fluid* | 50 | 36 (72%) | 70 | 61 (87%)<br>*31*<br>*30* | 9 (13%)<br>*3*<br>*6* |

**Table 2.** List of metabolites identified and quantified in blastocoelic liquid and uterine fluid

| Compound | HMDB | KEGG | Main associated pathway |
|---|---|---|---|
| Alanine | HMDB00161 | C00041 | Alanine, aspartate and glutamate metabolism |
| Aspartate | HMDB00191 | C00049 | Alanine, aspartate and glutamate metabolism |
| Asparagine | HMDB00168 | C00152 | Alanine, aspartate and glutamate metabolism |
| Glutamate | HMDB03339 | C00217 | Alanine, aspartate and glutamate metabolism |
| Methionine | HMDB00696 | C00073 | Cysteine and methionine metabolism |
| Dimethylsulfone | HMDB04983 | C11142 | Cysteine and methionine metabolism |
| Tyrosine | HMDB00158 | C00082 | Tyrosine metabolism |
| Valine | HMDB00883 | C00183 | Leucine, isoleucine, valine metabolism |
| 3-hydroxyisobutyrate | HMDB00023 | C06001 | Leucine, isoleucine, valine metabolism |
| 3-methyl-2-oxovalerate | HMDB00491 | C03465 | Leucine, isoleucine, valine metabolism |
| Creatine | HMDB00064 | C00300 | Glycine, serine and threonine metabolism |
| Beta-alanine | HMDB00056 | C00099 | Pyrimidine metabolism |
| Glucose | HMDB00122 | C00031 | Glycolysis/gluconeogenesis |
| Pyruvate | HMDB00243 | C00022 | Glycolysis/gluconeogenesis |
| Citrate | HMDB00094 | C00158 | Citrate cycle (TCA cycle) |
| Succinate | HMDB00254 | C00042 | Citrate cycle (TCA cycle) |
| 2-oxoglutarate | HMDB00208 | C00026 | Citrate cycle (TCA cycle) |
| Fumarate | HMDB00134 | C00122 | Citrate cycle (TCA cycle) |
| Choline | HMDB00097 | C00114 | Glycerophospholipid metabolism |
| o-acetylcholine | HMDB00895 | C01996 | Glycerophospholipid metabolism |
| Ethanolamine | HMDB00149 | C00189 | Glycerophospholipid metabolism |
| Malonate | HMDB00691 | C00383 | Fatty acid biosynthesis |
| Dimethylamine | HMDB00087 | C00543 | Methane metabolism |
| 2-phenylpropionate | HMDB11743 | | |

Metabolome analysis of blastocoelic and uterine fluids identified 69 spectral bins. Among those, 24 metabolites were identified, including amino acids (alanine, aspartate, asparagine, glutamate, methionine, tyrosine, valine), organic acids (citrate, pyruvate, succinate), and organic compounds (3-hydroxyisobutyrate, 3-methyl-2-oxovalerate, 2-oxoglutarate, 2-phenylpropionate, acetylcholine, beta-alanine, creatine, dimethylamine, dimethylsulfone, choline, ethanolamine, fumarate, glucose, malonate) (Table 2). These metabolites were associated with KEGG pathways including five amino acid metabolism pathways, pyrimidine metabolism pathways, glycolysis/gluconeogenesis, tricarboxylic acid (TCA) cycle, glycerophospholipid metabolism, fatty acid biosynthesis, and methane metabolism pathways (Table 2). Table 3 shows the concentration of each identified metabolite from blastocoelic and uterine fluids and the difference in concentrations between fluids. Identified metabolites were mainly more concentrated in uterine fluid than in blastocoelic fluid, except for pyruvate (Table 3). Aspartate and glutamate concentrations were detectable only in blastocoelic fluid, unlike tyrosine that was detectable only in uterine fluids (Table 3). Blastocoelic fluid contains mostly alanine, glutamate, glucose, and pyruvate and uterine fluid contains mostly alanine, glucose, and pyruvate (Table 3). The quality of the spectra was not sufficient to correctly identify and quantify leucine, isoleucine, acetate, lactate, and threonine.

To determine the overall metabolic convergence/difference between blastocoelic and uterine fluids, the $^{1}$H-NMR spectra and the metabolite concentrations were processed by PCA (Figure 5A and C) and PLS-DA (Figure 5B and D). PCA is an unsupervised method allowing the visualization of similarities or discrepancies in the datasets without any prior knowledge of sample classes. PCA of $^{1}$H-NMR spectra differentiated two clusters according to fluid type; the first two principal components explained 44.1% of the total variances (Figure 5A). Using metabolite concentrations, PCA also differentiated two clusters according to fluid type; the first two principal components explained 48.4% of the total variances (Figure 5C). In contrast to PCA, PLS-DA analysis takes advantage of class information in order to maximize the separation between groups. Indeed, PLS-DA improved the analysis, as the model displayed a good separation between blastocoelic and uterine fluids using spectra (Accuracy = 0.93; $R^2$ = 0.82; $Q^2$ = 0.62) (Figure 5B) and using metabolite concentrations (Accuracy = 0.93; $R^2$ = 0.97; $Q^2$ = 0.74) (Figure 5D). Thus, both the global analyses using PCA and PLS-DA showed differences in the $^{1}$H-NMR spectra and in the metabolite concentrations according to fluid type.

## Discussion

In this work, an original strategy was developed to study both blastocoelic and uterine fluids from in vivo peri-implantation rabbit embryos. $^{1}$H-NMR spectroscopy metabolic profiles were performed in the collected fluids. Globally, out of 24 detected metabolites, 21 were detected in both fluids. Metabolites were mostly more concentrated in uterine fluids compared to blastocoel. The high concentration of glucose and pyruvate in the blastocoelic fluids demonstrated the seminal role of these energy sources in blastocyst development in vivo. Interestingly, the acidic amino acids (glutamate and aspartate) were not quantifiable in uterine fluids, in contrast to blastocoelic fluids, suggesting a local regulation of uterine fluid composition. To our knowledge, this is the first report of simultaneous analysis of blastocoelic and uterine fluids at the time of implantation in vivo in mammals.

The rabbit peri-implantation embryo was visualized on 7 days-post-coïtum (dpc), using high-resolution ultrasound biomicroscopy.

**Table 3.** Concentration of identified compounds in blastocoelic ($n = 7$) and uterine fluids ($n = 7$)

| Identified compound | Concentration in µM | | Wilcoxon rank sum test |
|---|---|---|---|
| | Blastocoelic fluid | Uterine fluid | |
| Alanine | 4519.1 ± 274.9 | 4684.7 ± 432.2 | ns |
| Aspartate | 290.2 ± 16.6 | nd | - |
| Asparagine | 442.4 ± 37.9 | 554.1 ± 50.4 | $P < 0.05$ |
| Glutamate | 1046.5 ± 65.1 | nd | - |
| Methionine | 382.6 ± 30.4 | 522.9 ± 39.5 | ns |
| Dimethylsulfone | 77.8 ± 11.6 | 84.4 ± 13.7 | ns |
| Tyrosine | nd | 118.4 ± 9.0 | - |
| Valine | 178.5 ± 19.7 | 216.0 ± 19.0 | $P < 0.05$ |
| 3-hydroxyisobutyrate | 48.0 ± 7.7 | 68.0 ± 6.8 | $P < 0.05$ |
| 3-methyl-2-oxovalerate | 30.6 ± 7.5 | 67.1 ± 9.3 | $P < 0.05$ |
| Creatine | 151.0 ± 8.2 | 183.9 ± 10.3 | ns |
| Beta-alanine | 100.9 ± 12.1 | 131.8 ± 8.6 | $P < 0.05$ |
| Glucose | 2595.2 ± 168.4 | 2926.3 ± 278.0 | ns |
| Pyruvate | 1398.1 ± 88.0 | 1088.4 ± 112.7 | $P < 0.05$ |
| Citrate | 165.3 ± 20.8 | 250.9 ± 17.4 | $P < 0.05$ |
| Succinate | 72.3 ± 4.4 | 106.2 ± 8.5 | $P < 0.05$ |
| 2-oxoglutarate | 200.8 ± 26.5 | 374.0 ± 39.6 | $P < 0.05$ |
| Fumarate | 37.5 ± 3.0 | 40.4 ± 3.6 | ns |
| Choline | 16.9 ± 3.0 | 27.1 ± 1.9 | $P < 0.05$ |
| o-acetylcholine | 66.3 ± 10.0 | 126.1 ± 11.9 | $P < 0.05$ |
| Ethanolamine | 139.9 ± 16.3 | 287.4 ± 54.7 | $P < 0.05$ |
| Malonate | 27.0 ± 7.8 | 63.5 ± 8.4 | $P < 0.05$ |
| Dimethylamine | 11.0 ± 2.5 | 26.1 ± 2.6 | $P < 0.05$ |
| 2-phenylpropionate | 136.8 ± 17.9 | 223.1 ± 21.1 | $P < 0.05$ |

Values are expressed as mean ± SEM. nd, no detection; ns, not significant.

We observed fluid-filled anechoic embryonic vesicles tightly surrounded by the maternal endometrium. For approximately one third of the studied embryos, the uterine cavity was clearly visualized between the blastocyst and the mesometrial region of the uterus. We never observed fluid spaces between the blastocyst and the antimesometrial side of the uterus, suggesting that apposition was effectively taking place on the antimesometrial side. These observations are consistent with histological studies describing that the initial contact and the point of first attachment are antimesometrial at the opposite side of the embryonic disc on 7 dpc [38–40]. Attachment occurs in restricted areas, called knobs, where trophoblast-uterine cell fusion occurs [41]. Uterine secretions subsequently appear between uterine epithelium and TE on the embryonic disc side, and then, the final chorioallantoic placenta develops [42].

In 15% of the visualized embryonic vesicles, one or two small hypoechogenic circles were observed in the embryonic disk area, appearing to be an accumulation of fluid between two layers. In rabbits, gastrulation starts before implantation, at 6 dpc [37]. Seven gastrulation stages have been identified. Stage 4 is characterized by the appearance of the Hensen's node at the tip of the primitive streak and coincides with the time when implantation starts at 7 dpc [37]. In stage 4 embryos, mesoderm cells start to migrate and ingress between hypoblast and epiblast, inducing a disconnection between these two layers [43]. Thus, we hypothesize that the small hypoechogenic areas we observed could correspond to the visualization of the detachment of hypoblast and epiblast layers.

One third of the embryonic vesicles observed were not perfectly spherical, but more or less deflated. In many species, dynamic collapse and re-expansion of the cavity are frequently observed in cultured blastocysts before hatching [44]. To our knowledge, the occurrence of these contractions in vivo has not been described. It cannot be excluded that this deflation might be induced by the experimental protocol. Indeed, embryonic vesicles could have been subjected to osmotic and hydrostatic imbalances and temperature variations inducing fluid movements [45].

In the present work, the objective was to use ultrasound biomicroscopy-guided puncture to collect uterine and embryonic fluids in vivo. So far, most analyses to characterize oviductal or uterine fluids have been performed using postmortem samples collected on flushed reproductive tracts [46]. Postmortem hypoxia induces cell death and degradation products can be found in fluids after flushing and squeezing. Flushing induces dilution difficult to take into account and does not make it possible to characterize the juxta-embryonic uterine microenvironment [46].

$^{1}$H-NMR spectroscopy was used to determine metabolomic profiles of blastocoelic and uterine fluids. Not knowing the impact of deflation on these fluids composition, we only profiled samples from fully inflated, noncollapsed embryos. $^{1}$H-NMR spectroscopy is a robust metabolomics technique to identify and quantify low-molecular-weight compounds [47]. It is widely used to determine global metabolites profiles in biofluids and to noninvasively identify biomarkers in diseases [48]. In embryo biotechnology in reproductive medicine, $^{1}$H-NMR has been primarily used for identifying biomarkers in embryo culture media [5, 49]. So far, metabolomic studies of blastocoelic fluid are scarce and were not performed in vivo. One study reports on carbohydrate and amino acid contents in the blastocoel composition of in vitro produced bovine embryos [50]. Liquid chromatography and mass

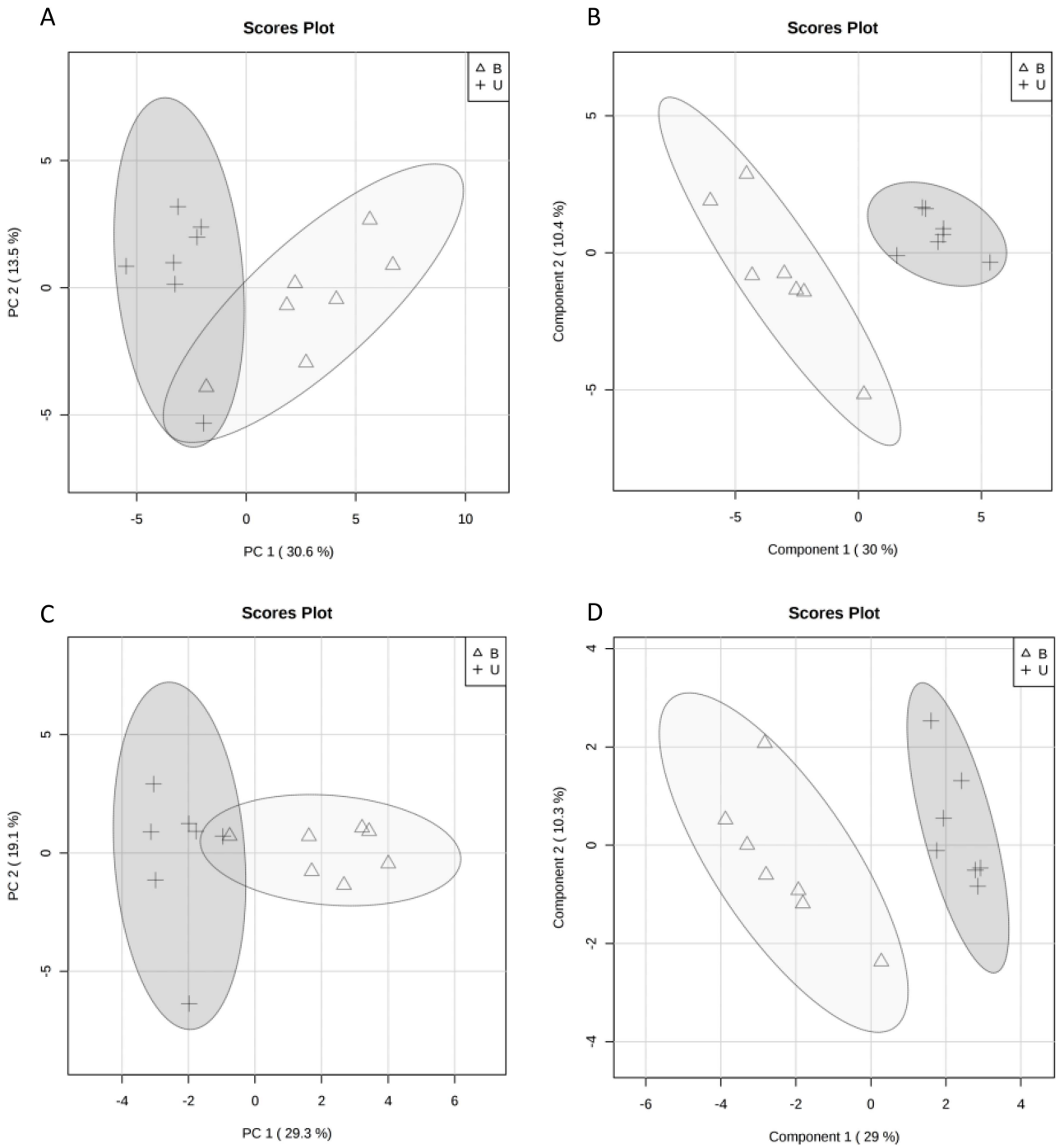


**Figure 5.** Multivariate statistical data analysis of blastocoelic (Δ B) and uterine (+ U) $^{1}$H NMR spectra (A and B) or metabolite concentrations (C and D) using unsupervised PCA (A and C) or supervised partial least squares discriminant analysis (B and D).

spectrometry were used to determine the impact of maternal diabetes on the blastocoelic fluid in ex vivo rabbit embryos (developed in vivo and recovered by uterine flush on 6 dpc) [51]. A large number of metabolites were detected, but not quantified, in this very comprehensive study [51]. In terms of uterine fluids, more data are available in humans and in other animal models [21, 23–25]. These data are limited due to the diversity of studied maternal conditions and to the fact that they reflect the main composition of the fluids but not the local microenvironment surrounding the embryo influenced by the embryo [21, 23, 46, 52]. The present study aimed at deciphering the environment in the immediate vicinity of the implanting embryo.

In blastocoelic and uterine fluids, more than 20 metabolites were identified, including nutrients such as carbohydrates and amino acids. In terms of carbohydrates, glucose and pyruvate were detected at the highest concentrations. The mammalian blastocyst has an important capacity to use glucose as an energy source, in contrast to early embryos [53]. In both blastocoelic and uterine fluids, glucose

was detected at equal concentrations, higher than those reported in the literature, i.e., in blastocoelic fluids of in vitro bovine embryos [50] and in uterine fluids of nonpregnant mice [54, 55], rabbits [56] or women [48]. Glucose is derived from the reproductive tract and is transported across membranes mainly using non-insulin-dependent facilitated glucose transporters [25, 53, 57]. Pyruvate was also present in both blastocoelic and uterine fluids at concentrations close to those of glucose. As for glucose, pyruvate concentrations were higher than those reported in blastocoelic and uterine fluids from mice or nonpregnant women [48, 50, 54, 55]. Pyruvate is essential for the early development of the preimplantation embryo [58]. Exogenous pyruvate originates from the uterine fluid and is subjected to a facilitated transport to embryo using monocarboxylate cotransporter [53, 59]. With the increasing demand of glucose to reach the blastocyst stage, the current understanding is that glucose becomes the primary energy source, through glycolysis, at the blastocyst stage and that pyruvate is not essential any more at this stage [53]. Very recently, however, the need for glucose to achieve compaction and cavitation in mouse embryos was shown to rely on glycolysis-independent glucose metabolism [58]. In mice, glucose is critically important for progression to the blastocyst stage by controlling the TE cell fate through hexosamine biosynthetic and pentose phosphate pathways but exogenous pyruvate continues to contribute to the TCA and to represent the main source of energy for the blastocyst [58]. In the present study, pyruvate was detected in the uterine fluid at a lower concentration than in the blastocoel. Moreover, TCA intermediates such as citrate, succinate, 2-oxoglutarate, and fumarate were detected at lower concentrations in the blastocoelic fluid than in the uterine fluid. High pyruvate and low TCA intermediates may reflect low pyruvate feeding to Krebs cycle [53]. Unfortunately, lactate could not be detected due to spectral defect and the pyruvate/lactate ratio could not be determined [53].

Amino acids act as source of energy and they are crucial for optimal development in preimplantation embryos. They are used for protein synthesis and play a role in osmoregulation and in the regulation of intracellular pH buffer [60]. The mammalian blastocyst possesses several transporters for amino acids [61, 62]. Alanine, the most concentrated metabolite detected, was present at similar concentrations in uterine and blastocoelic fluids. Alanine is present in high concentrations in oviductal and uterine fluids in human [63], mouse [54], bovine [55], and rabbit [64]. It is transported across the TE through system $B^{0,+}$ [62] and has also been detected in the blastocoel of ex vivo rabbit [64] and in vitro produced bovine embryos [50]. In vitro studies in the bovine species have highlighted an embryonic production of alanine both by ICM and TE, suggesting that alanine detected in blastocoelic and uterine fluids could have an embryonic origin [50]. Alanine regulates pH and plays an important role in the detoxification of ammonia generated by amino acid metabolism [65, 66].

Glutamate and aspartate were detected in blastocoelic fluids in concentrations consistent with that previously described in blastocoelic fluids of in vitro bovine embryos [50]. Surprisingly, glutamate and aspartate were not detected in uterine fluids. In contrast, both were shown to be present in the uterine fluids of nonpregnant women [63] and also in rats [46], mice [67], and heifers [68] around implantation. Although it cannot be excluded that the lack of detection in uterine fluids may be due to sensitivity limitations, it could be hypothesized that glutamate and aspartate detected in the blastocoel are endogenous products. A reduction in glutamate and aspartate concentrations at the time of implantation has been highlighted in the mouse blastocyst [69]. Since in the present study, only the microenvironment was analyzed, a local variation in the aspartate and glutamate transport systems activities might explain the observed results [69]. Aspartate and glutamate being acidic amino acids, these local changes could contribute to local pH variations, reported in other species to be mainly induced by lactate, to favor implantation [69, 70]. Nevertheless, it cannot so far be excluded that this is a species-specific phenomenon.

Creatine, a substrate for amino acid production and an energy reservoir, has been detected in both blastocoelic and uterine fluids. Creatine has been detected in the rabbit [71] and mouse blastocyst [72], in rabbit embryo blastocoelic fluid [51], and in the reproductive tract fluid in mice [73] and cattle [74]. Creatine kinase, the enzyme involved in the conversion of creatine to phosphocreatine and inversely, has been detected in rabbit and mouse blastocysts [71, 72]. Finally, tyrosine was detected at low concentrations in uterine fluid but was not identified in the blastocoelic fluid. As tyrosine was shown to be present at lesser concentrations in blastocoelic fluids compared to uterine fluids in bovine [50] and rabbit [64] embryos, this lack of detection may be due to sensitivity limitations in the present case.

In conclusion, by developing an innovative technique coupling ultrasound biomicroscopy, guided puncture, and NMR, the preimplantation embryo was visualized in vivo in its microenvironment, and both intra- and extra-embryonic fluids were collected and analyzed. The in vivo visualization of the implanting embryo confirmed previously described developmental stages based on histological observations but also provided further precision on the timing and localization of events. Further use of this technology in rabbits or other species could improve our understanding of anatomical events occurring during implantation. Further optimization of the technique, such as adjusting fluid volume collection and reducing the duration of surgery and genital tract externalization, could help improve fetal survival, as survival was only partial at 18 dpc (data not shown). Metabolomic analyses first highlighted the potential importance of pyruvate for the implanting blastocyst and underlined the necessity for studying the local embryo environment and interactions with the endometrium. Indeed, a better understanding of local regulations may provide seminal information for the refinement of ART. The methods developed here for the first time in the rabbit model could be implemented in other species and also allow other analyses, including proteomic, lipidomic, and microvesicle investigations.

## Supplementary Material

Supplementary material is available at *BIOLRE* online.

## Author contributions

SC, ND, EM, CR, FL, CM, GR, PC-P, and VD designed the study. SC, ND, EM, CR, MD, FL, and JG performed the research. SC, ND, EM, CR, JG, and LN-D analyzed the data. SC, PC-P, and VD wrote the paper.

## Acknowledgments

We thank staff from the INRAE animal experimentation unit (UE1298—SAAJ, INRAE Jouy-en-Josas, France) and MIMA2 (MIMA2, Microscopy

and Imaging Facility for Microbes, Animals and Foods, https://doi.org/10.15454/1.5572348210007727E12).

**Conflict of Interest**: The authors have no conflict of interest.

## References


1. De Geyter C, Calhaz-Jorge C, Kupka MS, Wyns C, Mocanu E, Motrenko T, Scaravelli G, Smeenk J, Vidakovic S, Goossens V, Gliozheni O, Hambartsoumian E et al. ART in Europe, 2015: Results generated from European registries by ESHRE. *Hum Reprod Open* 2020; **2020**:1–17.
2. Nyboe Andersen A, Goossens V, Bhattacharya S, Ferraretti AP, Kupka MS, de Mouzon J, Nygren KG, European IVF-monitoring (EIM) Consortium, for the European Society of Human Reproduction and Embryology (ESHRE). Assisted reproductive technology and intrauterine inseminations in Europe, 2005: Results generated from European registers by ESHRE: ESHRE. The European IVF monitoring programme (EIM), for the European Society of Human Reproduction and Embryology (ESHRE). *Hum Reprod* 2009; **24**:1267–1287.
3. Armstrong S, Bhide P, Jordan V, Pacey A, Farquhar C. Time-lapse systems for embryo incubation and assessment in assisted reproduction. *Cochrane Database Syst Rev* 2018; **5**:CD011320.
4. Hernández-Vargas P, Muñoz M, Domínguez F. Identifying biomarkers for predicting successful embryo implantation: Applying single to multi-OMICs to improve reproductive outcomes. *Hum Reprod Update* 2020; **26**:264–301.
5. Bracewell-Milnes T, Saso S, Abdalla H, Nikolau D, Norman-Taylor J, Johnson M, Holmes E, Thum M-Y. Metabolomics as a tool to identify biomarkers to predict and improve outcomes in reproductive medicine: a systematic review. *Hum Reprod Update* 2017; **23**:723–736.
6. Rødgaard T, Heegaard PMH, Callesen H. Non-invasive assessment of in-vitro embryo quality to improve transfer success. *Reprod Biomed Online* 2015; **31**:585–592.
7. Poli M, Ori A, Child T, Jaroudi S, Spath K, Beck M, Wells D. Characterization and quantification of proteins secreted by single human embryos prior to implantation. *EMBO Mol Med* 2015; **7**:1465–1479.
8. Jensen PL, Beck HC, Petersen J, Hreinsson J, Wånggren K, Laursen SB, Sørensen PD, Christensen ST, Andersen CY. Proteomic analysis of human blastocoel fluid and blastocyst cells. *Stem Cells Dev* 2013; **22**:1126–1135.
9. D'Alessandro A, Federica G, Palini S, Bulletti C, Zolla L. A mass spectrometry-based targeted metabolomics strategy of human blastocoele fluid: a promising tool in fertility research. *Mol Biosyst* 2012; **8**:953–958.
10. Tedeschi G, Albani E, Borroni EM, Parini V, Brucculeri AM, Maffioli E, Negri A, Nonnis S, Maccarrone M, Levi-Setti PE. Proteomic profile of maternal-aged blastocoel fluid suggests a novel role for ubiquitin system in blastocyst quality. *J Assist Reprod Genet* 2017; **34**:225–238.
11. Rienzi L, Gracia C, Maggiulli R, LaBarbera AR, Kaser DJ, Ubaldi FM, Vanderpoel S, Racowsky C. Oocyte, embryo and blastocyst cryopreservation in ART: systematic review and meta-analysis comparing slow-freezing versus vitrification to produce evidence for the development of global guidance. *Hum Reprod Update* 2017; **23**:139–155.
12. Boyard J, Reignier A, Chtourou S, Lefebvre T, Barrière P, Fréour T. Should artificial shrinkage be performed prior to blastocyst vitrification? A systematic review of the literature and meta-analysis. *Hum Fertil* 2020; **0**:1–9.
13. Nagy ZP, Shapiro D, Chang C-C. Vitrification of the human embryo: A more efficient and safer in vitro fertilization treatment. *Fertil Steril* 2020; **113**:241–247.
14. De Paepe C, Krivega M, Cauffman G, Geens M, Van de Velde H. Totipotency and lineage segregation in the human embryo. *Mol Hum Reprod* 2014; **20**:599–618.
15. Wu G, Schöler HR. Chapter Seventeen - Lineage segregation in the totipotent embryo. In: Wassarman PM (ed.), *Current Topics in Developmental Biology*, vol. **117**. Academic Press; 2016: 301–317.
16. Watson AJ, Barcroft LC. Regulation of blastocyst formation. *Front Biosci J Virtual Libr* 2001; **6**:D708–D730.
17. Robinson DH, Benos DJ. Chapter 4 Ion and solute transport in preimplantation mammalian embryos. In: Benos DJ (ed.), *Current Topics in Membranes*, vol. **39**. San Diego: Academic Press; 1991: 121–150.
18. Dardik A, Schultz RM. Protein secretion by the mouse blastocyst: Differences in the polypeptide composition secreted into the blastocoel and medium. *Biol Reprod* 1991; **45**:328–333.
19. Li S, Winuthayanon W. Oviduct: roles in fertilization and early embryo development. *J Endocrinol* 2017; **232**:R1–R26.
20. Leese HJ, Tay JI, Reischl J, Downing SJ. Formation of fallopian tubal fluid: role of a neglected epithelium. *Reprod Camb Engl* 2001; **121**:339–346.
21. Zhang Y, Wang H, Duan E. Uterine fluid in pregnancy: a biological and clinical outlook. *Trends Mol Med* 2017; **23**:604–614.
22. Pérez-Cerezales S, Ramos-Ibeas P, Acuña OS, Avilés M, Coy P, Rizos D, Gutiérrez-Adán A. The oviduct: from sperm selection to the epigenetic landscape of the embryo. *Biol Reprod* 2018; **98**:262–276.
23. Yang Y, Wang L, Chen C, Qi H, Baker PN, Liu X, Zhang H, Han T-L. Metabolic changes of maternal uterine fluid, uterus, and plasma during the peri-implantation period of early pregnancy in mice. *Reprod Sci Thousand Oaks Calif* 2020; **27**:488–502.
24. Gardner DK, Lane M, Calderon I, Leeton J. Environment of the preimplantation human embryo in vivo: metabolite analysis of oviduct and uterine fluids and metabolism of cumulus cells. *Fertil Steril* 1996; **65**:349–353.
25. Hu K, Yu Y. Metabolite availability as a window to view the early embryo microenvironment in vivo. *Mol Reprod Dev* 2017; **84**:1027–1038.
26. Foster FS, Pavlin CJ, Harasiewicz KA, Christopher DA, Turnbull DH. Advances in ultrasound biomicroscopy. *Ultrasound Med Biol* 2000; **26**:1–27.
27. Foster FS, Hossack J, Adamson SL. Micro-ultrasound for preclinical imaging. *Interface Focus* 2011; **1**:576–601.
28. Turnbull DH, Bloomfield TS, Baldwin HS, Foster FS, Joyner AL. Ultrasound backscatter microscope analysis of early mouse embryonic brain development. *Proc Natl Acad Sci U S A* 1995; **92**:2239–2243.
29. Zhou YQ, Foster FS, Qu DW, Zhang M, Harasiewicz KA, Adamson SL. Applications for multifrequency ultrasound biomicroscopy in mice from implantation to adulthood. *Physiol Genomics* 2002; **10**:113–126.
30. Mu J, Slevin JC, Qu D, McCormick S, Adamson SL. In vivo quantification of embryonic and placental growth during gestation in mice using micro-ultrasound. *Reprod Biol Endocrinol RBE* 2008; **6**:34.
31. Nieman BJ, Turnbull DH. Ultrasound and magnetic resonance microimaging of mouse development. *Methods Enzymol* 2010; **476**:379–400.
32. Liu A, Joyner AL, Turnbull DH. Alteration of limb and brain patterning in early mouse embryos by ultrasound-guided injection of Shh-expressing cells. *Mech Dev* 1998; **75**:107–115.
33. Domínguez-Bendala J, Álvarez-Cubela S, Nieto M, Vargas N, Espino-Grosso P, Sacher VY, Pileggi A, García E, Ricordi C, Inverardi L, Pastori RL. Intracardial embryonic delivery of developmental modifiers in utero. *Cold Spring Harb Protoc* 2012; **2012**:962–968.
34. Punzo C, Cepko CL. Ultrasound-guided in utero injections allow studies of the development and function of the eye. *Dev Dyn* 2008; **237**:1034–1042.
35. Henriques-Coelho T, Gonzaga S, Endo M, Zoltick PW, Davey M, Leite-Moreira AF, Correia-Pinto J, Flake AW. Targeted gene transfer to fetal rat lung interstitium by ultrasound-guided intrapulmonary injection. *Mol Ther J Am Soc Gene Ther* 2007; **15**:340–347.
36. Wang G, Williamson R, Mueller G, Thomas P, Davidson BL, Jr PBM. Ultrasound-guided gene transfer to hepatocytes in utero. *Fetal Diagn Ther* 1998; **13**:197–205.
37. Fischer B, Chavatte-Palmer P, Viebahn C, Navarrete Santos A, Duranthon V. Rabbit as a reproductive model for human health. *Reprod Camb Engl* 2012; **144**:1–10.
38. Nishimura M. Timing of implantation in New Zealand White rabbits. *Congenit Anom* 2001; **41**:198–203.
39. Idkowiak J, Weisheit G, Plitzner J, Viebahn C. Hypoblast controls mesoderm generation and axial patterning in the gastrulating rabbit embryo. *Dev Genes Evol* 2004; **214**:591–605.
40. Idkowiak J, Weisheit G, Viebahn C. Polarity in the rabbit embryo. *Semin Cell Dev Biol* 2004; **15**:607–617.

41. Carson DD, Bagchi I, Dey SK, Enders AC, Fazleabas AT, Lessey BA, Yoshinaga K. Embryo implantation. *Dev Biol* 2000; **223**:217–237.
42. Pijnenborg R, Robertson WB, Brosens I, Dixon G. Review article: trophoblast invasion and the establishment of haemochorial placentation in man and laboratory animals. *Placenta* 1981; **2**:71–91.
43. Viebahn C, Stortz C, Mitchell SA, Blum M. Low proliferative and high migratory activity in the area of Brachyury expressing mesoderm progenitor cells in the gastrulating rabbit embryo. *Development* 2002; **129**:2355–2365.
44. Marcos J, Pérez-Albalá S, Mifsud A, Molla M, Landeras J, Meseguer M. Collapse of blastocysts is strongly related to lower implantation success: a time-lapse study. *Hum Reprod* 2015; **30**:2501–2508.
45. Chan CJ, Costanzo M, Ruiz-Herrero T, Mönke G, Petrie RJ, Bergert M, Diz-Muñoz A, Mahadevan L, Hiiragi T. Hydraulic control of mammalian embryo size and cell fate. *Nature* 2019; **571**:112–116.
46. Leese HJ, Hugentobler SA, Gray SM, Morris DG, Sturmey RG, Whitear S-L, Sreenan JM. Female reproductive tract fluids: Composition, mechanism of formation and potential role in the developmental origins of health and disease. *Reprod Fertil Dev* 2008; **20**:1–8.
47. Nicholson JK, Lindon JC, Holmes E. 'Metabonomics': understanding the metabolic responses of living systems to pathophysiological stimuli via multivariate statistical analysis of biological NMR spectroscopic data. *Xenobiotica Fate Foreign Compd Biol Syst* 1999; **29**: 1181–1189.
48. Silva RA, Pereira TCS, Souza AR, Ribeiro PR. 1H NMR-based metabolite profiling for biomarker identification. *Clin Chim Acta Int J Clin Chem* 2020; **502**:269–279.
49. Muñoz M, Gatien J, Salvetti P, Martín-González D, Carrocera S, Gómez E. Nuclear magnetic resonance analysis of female and male pre-hatching embryo metabolites at the embryo-maternal interface. *Metabolomics Off J Metabolomic Soc* 2020; **16**:47.
50. Gopichandran N, Leese HJ. Metabolic characterization of the bovine blastocyst, inner cell mass, trophectoderm and blastocoel fluid. *Reprod Camb Engl* 2003; **126**:299–308.
51. Schindler M, Pendzialek SM, Grybel K, Seeling T, Navarrete Santos A. Metabolic profiling in blastocoel fluid and blood plasma of diabetic rabbits. *Int J Mol Sci* 2020; **21**:919.
52. Velasquez LA, Maisey K, Fernandez R, Valdes D, Cardenas H, Imarai M, Delgado J, Aguilera J. Croxatto HB. PAF receptor and PAF acetylhydrolase expression in the endosalpinx of the human fallopian tube: possible role of embryo-derived PAF in the control of embryo transport to the uterus. *Hum Reprod* 2001; **16**:1583–1587.
53. Gardner DK, Harvey AJ. Blastocyst metabolism. *Reprod Fertil Dev* 2015; **27**:638–654.
54. Kelleher AM, Burns GW, Behura S, Wu G, Spencer TE. Uterine glands impact uterine receptivity, luminal fluid homeostasis and blastocyst implantation. *Sci Rep* 2016; **6**:38078.
55. Harris SE, Gopichandran N, Picton HM, Leese HJ, Orsi NM. Nutrient concentrations in murine follicular fluid and the female reproductive tract. *Theriogenology* 2005; **64**:992–1006.
56. Ramin N, Thieme R, Fischer S, Schindler M, Schmidt T, Fischer B, Navarrete Santos A. Maternal diabetes impairs gastrulation and insulin and IGF-I receptor expression in rabbit blastocysts. *Endocrinology* 2010; **151**:4158–4167.
57. Leppens-Luisier G, Urner F, Sakkas D. Facilitated glucose transporters play a crucial role throughout mouse preimplantation embryo development. *Hum Reprod* 2001; **16**:1229–1236.
58. Chi F, Sharpley MS, Nagaraj R, Roy SS, Banerjee U. Glycolysis-independent glucose metabolism distinguishes TE from ICM fate during mammalian embryogenesis. *Dev Cell* 2020; **53**:9–26.e4.
59. Butcher L, Coates A, Martin KL, Rutherford AJ, Leese HJ. Metabolism of pyruvate by the early human embryo. *Biol Reprod* 1998; **58**:1054–1056.
60. Sturmey RG, Brison DR, Leese HJ. Symposium: innovative techniques in human embryo viability assessment. Assessing embryo viability by measurement of amino acid turnover. *Reprod Biomed Online* 2008; **17**:486–496.
61. Van Winkle LJ. Amino acid transport regulation and early embryo development. *Biol Reprod* 2001; **64**:1–12.
62. Van Winkle LJ, Tesch JK, Shah A, Campione AL. System B0,+ amino acid transport regulates the penetration stage of blastocyst implantation with possible long-term developmental consequences through adulthood. *Hum Reprod Update* 2006; **12**:145–157.
63. Kermack AJ, Finn-Sell S, Cheong YC, Brook N, Eckert JJ, Macklon NS, Houghton FD. Amino acid composition of human uterine fluid: association with age, lifestyle and gynaecological pathology. *Hum Reprod* 2015; **30**:917–924.
64. Gürke J, Hirche F, Thieme R, Haucke E, Schindler M, Stangl GI, Fischer B, Navarrete Santos A. Maternal diabetes leads to adaptation in embryonic amino acid metabolism during early pregnancy. *PLoS One* 2015; **10**:e0127465.
65. Orsi NM, Leese HJ. Ammonium exposure and pyruvate affect the amino acid metabolism of bovine blastocysts in vitro. *Reproduction* 2004; **127**:131–140.
66. Humpherson PG, Leese HJ, Sturmey RG. Amino acid metabolism of the porcine blastocyst. *Theriogenology* 2005; **64**:1852–1866.
67. Eckert JJ, Porter R, Watkins AJ, Burt E, Brooks S, Leese HJ, Humpherson PG, Cameron IT, Fleming TP. Metabolic induction and early responses of mouse blastocyst developmental programming following maternal low protein diet affecting life-long health. *PLoS One* 2012; **7**:e52791.
68. Forde N, Simintiras CA, Sturmey R, Mamo S, Kelly AK, Spencer TE, Bazer FW, Lonergan P. Amino acids in the uterine luminal fluid reflects the temporal changes in transporter expression in the endometrium and conceptus during early pregnancy in cattle. *PLoS One* 2014; **9**:e100010.
69. Van Winkle LJ, Dickinson HR. Differences in amino acid content of preimplantation mouse embryos that develop in vitro versus in vivo: in vitro effects of five amino acids that are abundant in oviductal secretions. *Biol Reprod* 1995; **52**:96–104.
70. Gardner DK. Lactate production by the mammalian blastocyst: manipulating the microenvironment for uterine implantation and invasion? *BioEssays News Rev Mol Cell Dev Biol* 2015; **37**:364–371.
71. Mukherjee A, Dey SK, Sen Gupta J, Ramadoss CS, Dickmann Z. Regulatory enzymes of carbohydrate and energy metabolism in the rabbit blastocyst. *J Reprod Fertil* 1978; **53**:77–80.
72. Forsey KE, Ellis PJ, Sargent CA, Sturmey RG, Leese HJ. Expression and localization of creatine kinase in the preimplantation embryo. *Mol Reprod Dev* 2013; **80**:185–192.
73. Umehara T, Kawai T, Goto M, Richards JS, Shimada M. Creatine enhances the duration of sperm capacitation: a novel factor for improving in vitro fertilization with small numbers of sperm. *Hum Reprod* 2018; **33**:1117–1129.
74. Lamy J, Gatien J, Dubuisson F, Nadal-Desbarats L, Salvetti P, Mermillod P, Saint-Dizier M. Metabolomic profiling of bovine oviductal fluid across the oestrous cycle using proton nuclear magnetic resonance spectroscopy. *Reprod Fertil Dev* 2018; **30**:1021–1028.